A Real-time Approach to Optimal Energy-Consumption for Autonomous Underwater Vehicles in Unknown Time-Varying Flow Fields

Mario A. Jordán, and Jorge L. Bustamante

Abstract— **This paper concerns the estimation of optimal energy paths to dose power demands in autonomous underwater vehicles with the end to achieve maximal autonomy in the presence of a flow field. The trajectories searched for are parameterized and structured on a grid (usually employed in sampling missions on the sea bottom) with a relative orientation with respect to the current flow. The optimal solution is a set of cruise velocities along the path. A practical approach is developed in real time for accomplishing path corrections due to spurious in the flow. A theoretical background is developed and a simulation study is given with comparative optimal and suboptimal solutions.**

Keywords— **Optimal energy spent - Unmanned underwater vehicles - Time-varying Flow Field - Maximal autonomy - Energy optimization - Control systems.**

I. Introduction

A preventive analysis of power supply demands in the guidance of unmanned subaquatic vehicles is always evaluated as an important task when an inboard closed-energy system is employed like in the autonomous underwater vehicles. This scenario takes place above all when long navigation times or large run paths have to be fulfilled for a specific mission such as long data gathering. Additionally, the influence of currents in the fluid environment suggests a more critical trouble in the analysis [R. Blidberg, 2001].

It is well known that large cruise velocities in marine systems are associated with high energy consumptions. This is particularly more accentuated in subaquatic vehicles in where the motion resistance force increases about proportional to the square of the velocity. Even if the vehicle navigates at low rates of motion, the action of perturbations like currents may influence the demand of energy during more extensive periods causing ultimately the exhaustion of the reserve with relatively shorter run paths than those expected [Woodrow *et. al*, 2005].

When maximal autonomy is search for planned missions, the anticipated calculation of a "point of no return" of an autonomous vehicle is a desired task mainly for security reasons. This involves practical the estimation of optimal trajectories minimizing time, energy, maximizing length of the path, or combination of them [Chyba *et al.*, 2009]

In this paper we focus two important practical cases for AUVs (autonomous underwater vehicles). In the first one, a pipeline has to be tracked with inspection ends using camera with vision-based control or metal detector systems. In the second case, a region over the sea bottom has to be surveyed on transects and grid lines (see Fig. 1). A common feature of both cases is that the trajectory is somewhat fixed, however in the second case an optimal orientation should be given because of the direction of the flow field.

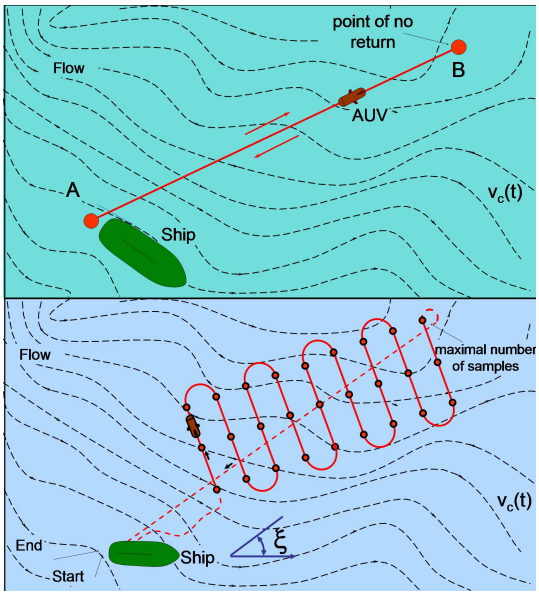

Fig. 1 - Navigation in a time-varying flow field. Top: Maximal autonomy in bidirectional path. Bottom: Maximal number of uniformly spread samples onto a grid

Another point which is not touched in the literature is the influence of the vehicle shape (usually torpedo form with quite distinct hydrodynamics coefficients in the main axes) in the energy consumption when the fluid flow acts from quite different directions other than from frontal side.

Finally, other related interesting scenarios can be found in missions with requirements on minimal navigation times. Such scenarios are generally motivated, for instance, by sampling missions in where the validity of the results rests on the constancy of experiment conditions in time. This may vary for instance with the tide and solar radiation periods.

On the contrary, we will depart from a real scenario which is to consider that the flow field is unknown and time-varying. This contrasts with the majority of the approaches found in the bibliography, which depart from the knowledge of current maps that will facilitate a global energy- or

Corresponding Author: Mario A. Jordán: E-mail: mjordan@criba.edu.ar. Address: CCT-CONICET. Florida 8000, B8000FWB, Bahía Blanca, ARGENTINA

Mario Jordán and Jorge Bustamante are with the Argentine Institute of Oceanography (IADO-CONICET) and Dto. de Ingeniería Eléctrica y de Computadoras (DIEC-UNS), Bahía Blanca, Argentina.

time-optimized vehicle motion. Additionally we postulate another useful fact that modern navigation systems do has the possibility of measuring the current as a local vector of flow field. Technologies sustained by the Acoustic Doppler Current Profilers (ADCP) or the Doppler Velocity Logs (DVL) support this fact.

Related present and past work has been posed in the context of the Maximum Principle of Pontryagin, with the goal to design a control strategy that generally searches for a vehicle trajectory that minimizes run time between two extreme positional and kinematical configuration sets [Chyba *et al.*, 2004]. Even if these optimal trajectories can be computed numerically based on a complete description of the vehicle dynamics, they are generally not implementable due to the multiple and rapid thrust switching required by the thrusters [Chyba and Haberkorn, 2005]. However, sacrificing the continuity of the solution and allowing the manipulated thrusts to evolve stepwise, a tolerable gap between this practical and the optimal solutions is achieved [Chyba *et al.*, 2008]. Finally, it is interesting that later a combination between minimal time and minimal energy consumption could be established and implemented, however in the practical sense pointed out above [Chyba *et al.*,2009].

One can also obtain substantially energy savings by actuating only a reduced set of motors or bypassing adverse currents and also exploiting favorable currents [Kruger *et al.*,2007]. Moreover, some approaches deal directly with the dynamics equation for choosing trajectories such that hydrodynamic drag on the system is reduced [Sarkar and Podder , 2001]. Other approaches generates directly the speed along the path based on energy of the ocean currents and a cost function containing information of inertia to speed up the convergence to the global minimum [Yang and Zhang, 2009].

The approach touched on in this work is different. It concerns the design of an algorithm to generate maximal run distance over an arbitrary parameterized and structured path for long data gathering. The motivation is to develop a practical approach in where corrections of optimal rate of the vehicle motion after changing perturbations (time-varying flow field) result in real-time implementations during the guidance along the path. A theoretical background is developed and a simulation study is given with comparative optimal and suboptimal solutions.

II. Problem description

A. Problem statement

We will posse the problem of optimal energy consumption to achieve maximal autonomy as

Initial conditions :

- Given a high-performance control system for guidance the unmanned underwater vehicle,
- the dynamics of the energy source (here batteries),
- an unknown uniform planar flow field $\mathbf{v}_c$=[v_{c_x},v_{c_y},0, 0,0,0]^T,
- an initial battery energy value $E_0 > 0$,
- a final battery energy value E_e with $E_0 > E_e \geq 0$ (here the energy reserve), and
- a spacial reference path $\boldsymbol{\eta}_{ref}(\xi)$ of a large length L, meandering uniformly over a prescribed grid like in Fig. 1, with ξ an unknown angle of the grid orientation,

Goal :

- then, one is interested in computing the control action to guide the vehicle from the start point of $\boldsymbol{\eta}_{ref}$ (point A in Fig. 1), reaching the largest run stretch $L_{\max} \leq L$ as possible (point B in Fig. 1) before to return to A again, beginning with E_0 up to empty out the energy to the low level E_e.

In our context of a sampling mission this goal means to allow the vehicle enter in the region of interest to gather the maximal number of samples as possible on a grid. Clearly $L_{\max}$ depends also on ξ.

Since we are thinking in a guidance control system with eventual unpredictable perturbations, possible solutions should have to be obtained in real time. The idea behind a high-performance controller will be clarified later.

B. Vehicle dynamics

We start from the dynamics of an underwater vehicle (cf. [Fossen,1994])

$$\dot{\mathbf{v}} = (M_b + M_a)^{-1}\Big(-C(\mathbf{v})\mathbf{v} - D(\mathbf{v}|)\mathbf{v} + \mathbf{g}(\boldsymbol{\eta}) + \boldsymbol{\tau}\Big) \quad (1)$$

$$\dot{\boldsymbol{\eta}} = J(\boldsymbol{\eta})(\mathbf{v} + v_c). \quad (2)$$

Herein $\boldsymbol{\eta} = [x, y, z, \phi, \theta, \psi]^T$ is the generalized position in an earth-fixed frame where the first three components describe translations and the remainder rotations. Additionally $\mathbf{v} = [u, v, w, p, q, r]^T$ is the generalized velocity vector in a vehicle-fixed frame where its components are the motion modes with respect to the main vehicle axes, namely: surge, sway, heave, pitch, roll and yaw, respectively. Moreover, J is the rotation matrix, M_b is the inertia matrix of the body and M_a is the additive mass of the surrounding fluid (the sum of both is referred to the inertia matrix M employed later), C the Coriolis matrix, D the nonlinear drag matrix, $\mathbf{g}$ is the restoration force and $\boldsymbol{\tau}$ the propulsion force considered as the manipulated variable in the control system. Finally $J(\boldsymbol{\eta})$ is the well-known rotation matrix depending on the angles ϕ, θ and ψ.

C. Autonomous navigation system

One starts the discussion in the framework of a path tracking problem accomplished by an autonomous navigation system whose elements are described in the Fig. 2. The controller builds up a generalized thrust $\boldsymbol{\tau}$ according to a feedback of the spatial and kinematic states $\boldsymbol{\eta}$ and $\mathbf{v}$, respectively in order to attenuate the respective path errors $\overset{\frown}{\boldsymbol{\eta}}$ and $\overset{\frown}{\mathbf{v}}$ with respect to the reference trajectories $\boldsymbol{\eta}_{ref}$ and $\mathbf{v}_{ref}$. The control algorithm includes a compensation of the thrusters dynamics, which are also dependent on the kinematic state [Healey *et al.*, 1995]. Finally the control action ends in the vector $\mathbf{n}_{ref}$ which are the rpm's on the thrusters to accomplish the control goal.

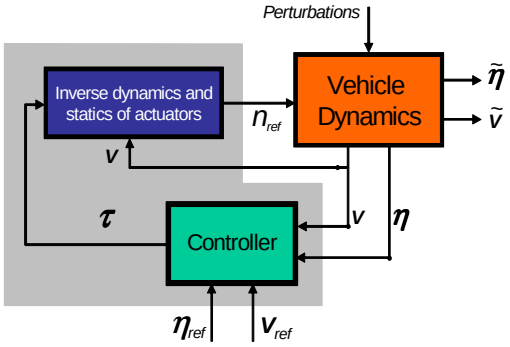

Fig. 2 - Control system for tracking of geometric and kynematic reference trajectories

It is important for further discussion to assume a high-performance controller. Such a controller would have to be able to attenuate $\hat{\boldsymbol{\eta}}$ and $\hat{\mathbf{v}}$ rapidly. A design that possesses this feature is developed in [Jordán and Bustamante, 2008].

Accordingly to this work, the tracking errors are defined as

$$\hat{\boldsymbol{\eta}}=\boldsymbol{\eta}-\boldsymbol{\eta}_{ref} \tag{3}$$

$$\hat{\mathbf{v}}=\mathbf{v}-J^{-1}(\boldsymbol{\eta})J(\boldsymbol{\eta}_{ref})\mathbf{v}_{ref}+J^{-1}(\boldsymbol{\eta})K_p\hat{\boldsymbol{\eta}}, \tag{4}$$

and the feedback vector (control action)

$$\boldsymbol{\tau}=C\mathbf{v}+D\mathbf{v}+\mathbf{g}+\mathbf{M}\left(\frac{\mathbf{d}}{\mathbf{dt}}(J^{-1}(\boldsymbol{\eta})\dot{\boldsymbol{\eta}}_{ref})-\frac{dJ^{-1}(\boldsymbol{\eta})}{dt}K_p\hat{\boldsymbol{\eta}}\right. \tag{5}$$

$$\left.+J^{-1}(\boldsymbol{\eta})K_p^2\hat{\boldsymbol{\eta}}-J^{-1}(\boldsymbol{\eta})K_pJ(\boldsymbol{\eta})\hat{\mathbf{v}}\right)-K_v\hat{\mathbf{v}}-J^T\hat{\boldsymbol{\eta}}.$$

So the path error system of Fig. 2 results in

$$\dot{\hat{\boldsymbol{\eta}}} = -K_p\hat{\boldsymbol{\eta}}+J\hat{\mathbf{v}}+J\ \mathbf{v}_c \tag{6}$$

$$\dot{\hat{\mathbf{v}}} = -M^{-1}K_v\hat{\mathbf{v}}-M^{-1}J^T\hat{\boldsymbol{\eta}}+J^{-1}K_pJ\mathbf{v}_c. \tag{7}$$

$$\mathbf{n}_{ref} = \mathbf{f}(\tau,v). \tag{8}$$

where $\mathbf{f}$ is a nonlinear function describing the static characteristic of the thrusters and $K_p \geq 0$ and $K_v \geq 0$ are design matrices in the controller [Jordán and Bustamante, 2008, 2009]. This control system is asymptotically stable in the space of $\boldsymbol{\eta}$ and $\mathbf{v}$ and is shown to be potentially be able to achieve a high performance.

D. Energy balance

One assumes the total energy available for the autonomous navigation is supplied internally by batteries and also eventually from the surrounding flow field. The more convenient vehicle orientation ξ to accomplish the route *A-B-A* is also a result of the intended optimization goal.

The energy in the batteries is subject to

$$E_b(t;\xi) = E_0-\int_{t_0}^{t} i_b(t;\xi)\ V_b\ d\tau = \tag{9}$$

$$= E_m+E_{ns}+E_{lb}+E_t$$

with i_b the battery supplied current and V_b the voltage, E_m is the mechanic energy of the vehicle motion, E_{ns} the energy spent by the vehicle motion and mission equipments, E_{lb} the energy lost in the battery and E_t is the thruster energy lost due to armature warm and drag effects at the thruster blades

The partial energies are

$$E_m(t;\xi) = \int_0^{\eta(t;\xi)} \boldsymbol{\tau}^T\ d\boldsymbol{\eta}=\int_0^t \boldsymbol{\tau}^T\ \mathbf{v}dt' \tag{10}$$

$$E_{ns}(t) = \int_0^t p_{ns}dt' = \bar{p}_{ns}\ t \tag{11}$$

$$E_{lb}(t) = E_0-\xi_b\int_0^t t\ dt' = E_0-\frac{\xi_b}{2}t^2 \tag{12}$$

$$E_t(t;\xi) = nR_t\int_0^t \mathbf{i}_t^2\ dt'+n\int_0^t \mathbf{f}_t^T\ \mathbf{v_t}\ dt'= \tag{13}$$

$$= \sum_{i=1}^{n}\int_0^t i_{t_i}\ V_t dt'- E_m(t;\xi), \tag{14}$$

where E_0 is the energy at the start point, R_t and i_t are the armature resistant and current, respectively, V_t is the voltage applied to the thruster, p_{ns} is the power needed for the operation of the equipments which is assumed constant and equal to $\bar{p}_{ns}$, ξ_b is a constant representing the leakage rate per time unit in the battery, n is the number of propellers, $\mathbf{v_t}$ is the traslational velocity vector projected onto every propeller axis and $\mathbf{f}_a$ is the drag force offered by fluid resistance at the thruster blades whose velocity through the blades is a nonlinear function of $\mathbf{v_t}$. Due to the difficulty of determining $\mathbf{f}_a$, Eq. (14) represents an alternative to (13) for computing E_t upon the armature currents i_{t_i} and the thruster voltage V_t.

III. Optimal solution

Let $\boldsymbol{\eta}(t)$ has the shape of a meandering path according to Fig. 1. It is valid

$$L(t) = \int_0^t \dot{\boldsymbol{\eta}}_{x,y,z}(t;\xi)dt' \tag{15}$$

with $\dot{\boldsymbol{\eta}}_{x,y,z}=[\dot{x},\dot{y},\dot{z}]^T$. It is noticing that $\dot{\boldsymbol{\eta}}_{x,y,z}$ and also $\boldsymbol{\eta}_{x,y,z}$ are optimal vectors in the direction ξ, where ξ is a parameter of the main course.

The optimal path is described by a velocity vector function $\mathbf{v}_{opt}(t) = J^{-1}(\boldsymbol{\eta}_{opt})\dot{\boldsymbol{\eta}}_{opt}(t)-\mathbf{v}_c$ that accomplish

$$\max_{\dot{\boldsymbol{\eta}}_{x,y,z},\ \xi} L(t) = L_{\max}, \tag{16}$$

with E_0 when $\boldsymbol{\eta}_{opt}(0)$ and E_e when the vehicle return to the start point with a rotations of 90 degrees per path corner.

In [Chyba et al., 2009] the approach suggested had consisted in calculating an optimal generalized force function $\boldsymbol{\tau}_{opt}(t)$ (i.e., the control action), we instead follow a different way consisting in defining directly the optimal course rate $\mathbf{v}_{opt}(t)$. This has the advantage of attaining approximative but implementable solutions.

First we conceived the geometric path $\boldsymbol{\eta}_{x,y,z}$ as composed by rectilinear stretches. We take advantage of the fact that the control system transients are originated mainly by course changes, it is, at a rotation points.

As the supposed controller has a wide frequency band, we can assume that the energy consumed during transients occurs in short periods referred to as ΔT.

In this way the lost energy during a transient is computed as

$$\Delta E_{b_{trans}}(t_t) = E_b(t_t+\Delta T) - E_b(t_t) = V_b \int_{t_t}^{t_t+\Delta T} i_b \, dt' - E_b(t_t), \tag{17}$$

with t_t an entrance time point to a new stretch. So $E_b(t)$ is a decreasing but not a continuous-time function. Outside the periods ΔT, the velocities on every rotation and stretch correspond to kinematic steady states.

The second consideration is that the steady state velocities are (practically close to) the reference velocities $\mathbf{v}_{ref}(t)$ on each stretch. So, we can compute the optimal thrust $\boldsymbol{\tau}_{opt}(t)$ indirectly by searching for the optimal set of constant $\mathbf{v}_{ref}(t)$ on every stretch and allowing the controller to force the advance rate $\mathbf{v}(t)$ to be close to $\mathbf{v}_{ref}(t)$. Simultaneously, an optimal direction ξ for the final meandering path must be established from this optimization procedure.

IV. Optimization procedure

Firstly we look at (10) and notice the incidence of the impulse thrust on the mechanic energy. Now, if we consider that the control system can achieve a good performance [Jordán and Bustamante, 2008, 2009] then control errors are approximately null and it is valid $\mathbf{v}_{ref} \approx \mathbf{v}$ and $\boldsymbol{\eta}_{ref} \approx \boldsymbol{\eta}$. Additionally, let the vehicle motion be also done with good regulations of the pitch and roll angles about fixed angles, so $J(\varphi, \theta)$ remains constant during the course. Then, we conclude from (5) that the generalized force $\boldsymbol{\tau}$ calculated by the controller depends approximately on the drag forces and buoyancy.

Another thing is that we can measure the local flow vector and so we can assume that this will remain constant in a vicinity of the measurement point.

It is worth noticing that the local measurement of the current will enable us to develop an optimization algorithm that can compute dynamically the optimal solution independently of the whole flow field. This implicates on the other side that the optimal control law is not known beforehand and is recalculated for the remainder path in real time. The amount of calculations to be done is also reduced by the fact that we contemplate a rate-based approach instead of a force-base approach as mentioned before.

Now, let us contemplate a planar path at constant depth. For every rectilinear stretch i including the rotation at the endpoint, the remainder energy is

$$\begin{aligned} E_i &= E_{i-1} - \Delta E_i - \bar{p}_{ns}\,(t_i - t_{i-1}) - \\ &\quad - \int_{t_{i-1}}^{t_i} c_x \,|u_i|\,(u_i)^2 \;\mathbf{dt'} - \int_{\mathbf{t_{i-1}}}^{\mathbf{t_i}} \mathbf{c_y}\,|\mathbf{v_i}|\,(\mathbf{v_i})^2 \;\mathbf{dt'} \end{aligned} \tag{18}$$

where u_i and v_i are the planar coordinates of $\mathbf{v}_{xy_i}$ which are measure locally at the step i and supposed the remain constant up to the step $i+1$. Additionally, ΔE_i sums up $\Delta E_{b_{trans}}$, E_{lb} and E_t together, and c_x and c_y represent coefficients of the drag forces in the direction x and y of the vehicle. The rotations about the end of the stretch points are computed separately.

Assuming a constant velocity $\mathbf{v}_{xy_i}$ and calculating from (18) the period taken for covering the length L_i one gets

$$L_i = \frac{E_{i-1} - \Delta E_i - E_i}{(\bar{p}_{ns} + c_x u_i^3 + c_y v_i^3)}\,(u_i + v_{c_i}) \tag{19}$$

with v_{c_i} the component of $\mathbf{v}_c$ on the advance direction on the stretch i. Thus

$$v_{c_i} = |\mathbf{v}_c|\cos(\xi) \tag{20}$$

$$v_i = |\mathbf{v}_c|\sin(\xi). \tag{21}$$

Considering now n stretches from the start point to the point of no return and n stretches for turning over to the start point, it is valid

$$L_1 = \frac{E_0 - \Delta E_1 - E_1}{(\bar{p}_{ns} + c_x u_1^3 + c_y v_1^3)}\,(u_1 + v_{c_1}) \tag{22}$$

$$L_2 = \frac{E_1 - \Delta E_2 - E_2}{(\bar{p}_{ns} + c_x u_2^3 + c_y v_2^3)}\,(u_2 + v_{c_2}) \tag{23}$$

.....

$$L_n = \frac{E_{n-1} - \Delta E_n - E_n}{(\bar{p}_{ns} + c_x u_n^3 + c_y v_n^3)}\,(u_n + v_{c_n}) \tag{24}$$

$$L_{n+1} = \frac{E_n - \Delta E_{n+1} - E_{n+1}}{(\bar{p}_{ns} + c_x u_{n+1}^3 + c_y v_{n+1}^3)}\,(u_{n+1} + v_{c_{n+1}}) \tag{25}$$

.....

$$L_{2n-1} = \frac{E_{2n-2} - \Delta E_{2n-1} - E_{2n-1}}{(\bar{p}_{ns} + c_x u_{2n-1}^3 + c_y v_{2n-1}^3)}\,(u_{2n-1} + v_{c_{2n-1}}) \tag{26}$$

$$L_{2n} = \frac{E_{2n-1} - \Delta E_{2n}}{(\bar{p}_{ns} + c_x u_{2n}^3 + c_y v_{2n}^3)}\,(u_{2n} + v_{c_{2n}}) \tag{27}$$

The stretches L_n and L_{n+1} are the same, however they may have different lengths that previous stretches. Moreover there are four different cases for the location of the point of no return (see Fig. 3).

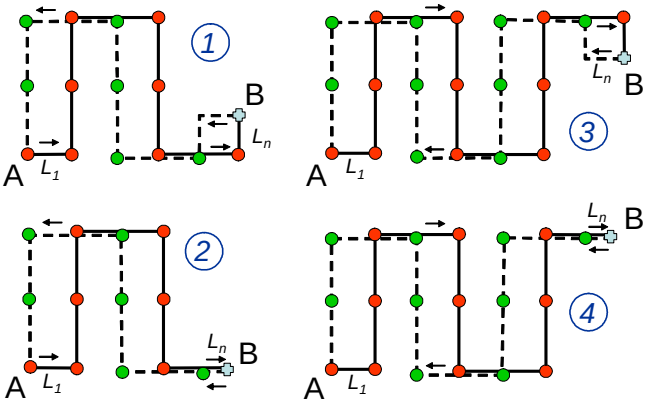

Fig. 3 - The four cases for the location of the point of no return (point B)

We are searching for a maximum of L_n. So with (24) and (25) and $L_n = L_{n+1}$ one attains

$$L_n = \frac{1}{2}\left(E_{n-1} - \Delta E_n - \Delta E_{n+1} - E_{n+1}\right) \left(\frac{(\bar{p}_{ns}+c_x u_{n+1}^3 + c_y v_{n+1}^3)}{(u_{n+1}+v_{c_{n+1}})} + \frac{(\bar{p}_{ns}+c_x u_n^3 + c_y v_n^3)}{(u_n+v_{c_n})}\right)^{-1}. \quad (28)$$

From (27) backwards we obtain E_{n+1} because with exception of $L_n = L_{n+1}$ the remainder lengths of the stretches are known from the structured path, for instance

$$E_{2n-1} = \frac{L_{2n}(\bar{p}_{ns}+c_x u_{2n}^3 + c_y v_{2n}^3)}{(u_{2n}+v_{c_{2n}})} + \Delta E_{2n}, \quad (29)$$

and in the same way from (19) forwards, one accomplishes an expression for E_{n-1} and so on up to

$$E_1 = E_0 - \Delta E_1 - \frac{L_1(\bar{p}_{ns}+c_x u_1^3 + c_y v_1^3)}{(u_1+v_{c_1})}. \quad (30)$$

For simplicity, the final energy $E_e = E_{2n} = 0$.

Finally L_n can be written as

$$L_n = \left(E_0 - \sum_{i=1}^{n-s}\Delta E_i - \sum_{i=n+2}^{n+s}\frac{L_i\left(\bar{p}_{ns}+c_x u_i^3 + c_y v_i^3\right)}{(u_i+v_{c_i})} - \sum_{i=1}^{n-1}\frac{L_i\left(\bar{p}_{ns}+c_x u_i^3 + c_y v_i^3\right)}{(u_i+v_{c_i})}\right) \left(\frac{(\bar{p}_{ns}+c_x u_{n+1}^3 + c_y v_{n+1}^3)}{(u_{n+1}+v_{c_{n+1}})} + \frac{(\bar{p}_{ns}+c_x u_n^3 + c_y v_n^3)}{(u_n+v_{c_n})}\right)^{-1} \quad (31)$$

Since L_n has a maximum with respect to the choice of the velocities u_i we obtain from $\frac{\partial L_n}{\partial u_i} = 0$ for $i = 1, ..., 2n$ the following restrictions

$$\bar{p}_{ns} + c_y v_i^3 - 2c u_i^3 - c3 v_i^2 v_{c_i} = 0 \quad (32)$$

One notices from (32) that the optimal velocity u_i in each stretch is independent of the velocities in the remainder stretches. Moreover So, the u_i´s can be calculated beforehand in order to know how many stretches will be covered with the available energy E_0 until achieving the maximal $L_n = L_{n+1}$ and finally obtaining $L = \sum_{i=1}^{2n} L_i$.

As the structured path is also parameterized in ξ, one sees that its course orientation influences the energy consumption in the presence of a flow field. This dependence is seen from (20)-(21) in (32).

The optimal ξ determines the ultimate path orientation. This is obtained from the condition $\frac{\partial L_n}{\partial \xi} = 0$. For reasons of conciseness, an analytical expression of this condition is not written out here. Conceptually this is an implicit nonlinear function with multiple maxima and minima (see Fig. 5 in the context of an example).

Hence, the optimal ξ to maximize L_n has to be attained numerically (for instance, using the Newton-Raphson Method) starting with an appropriate initial condition. Our experience is that $\xi_0 = \frac{\pi}{4}$ is a good start value.

The generalization of the algorithm for a three-dimensional velocity $\mathbf{v}_{xyz_i}$ is straightforward. This has sense when the altitude in motion is maintained constant over an irregular terrain. Finally, the inclusion of an energy reserve E_e implies simply to add $E_{2n} = E_e$ to the terms in the right hand of (29).

V. Vehicle guidance with energy optimization

The previous algorithm can be embedded in a navigation system as illustrated in Fig. 4. The new block conforms an outer loop and contains the real-time algorithm with optimal spent of energy along the proposed path in long-data gathering missions.

The block generates the optimal velocities u_i, which are associated to the kinematic reference $\mathbf{v}_{ref}$ for the controller. Also the optimal orientation of the path with respect to ξ gives the ultimate coordinates for the geometric reference $\boldsymbol{\eta}_{ref}$.

Basically the condition for stability of the nested loops is that $\dot{\boldsymbol{\eta}}_{ref}$ be bounded in every stretch. The proof falls outside the scope of this paper and pertains to the condition for the stability of the control system given in [Jordán and Bustamante, 2009].

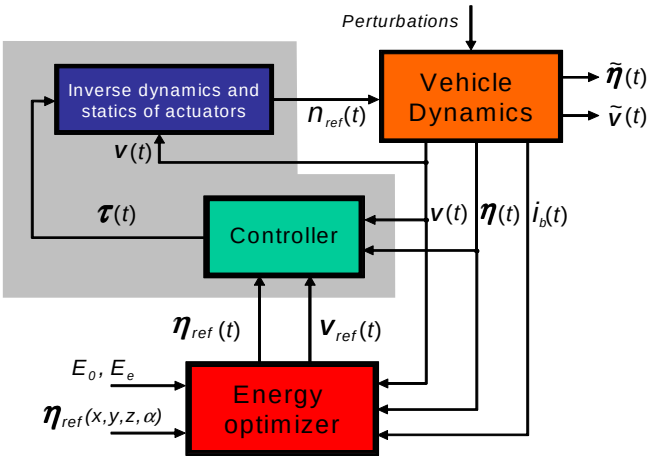

Fig. 4 - Nested control loops with energy optimizer

If the course and/or the intensity of the flow field change suddenly at a coordinate of the path, the remainder optimal velocities can be released and recalculated again with the available energy. The algorithm described here is time-saving and efficient that it can be applied in real-time with standard computational hardware.

VI. Case study

Let us now illustrate the features of the proposed algorithm according to a planar path with the structure depicted in Fig. 1, bottom. To this end, we start the case

study with the following setup

$$E_0 = 1.733 \text{ (MJ)} \qquad E_e = 0 \text{ (w)}$$
$$p_{ns} = 250 \text{ (w)} \qquad \Delta E_{trans} = 500 \text{ (J)}.$$
$$c_x = 120 \text{ (Kg/m)} \qquad c_y = 2400 \text{(Kg/m)}$$
$$\Delta X = 100 \text{ (m)} \qquad \Delta Y = 100 \text{ (m)}$$
$$|\mathbf{v}_c| = 0.2 \text{ (m/s)}$$

In Fig. 5 the variation of L with ξ obtained for the different angles by means of (22)-(27) and (32) is presented. In many simulations with different setups, the optimal orientation lays regularly close to $\frac{\pi}{4}$. In this case the value span of L is about of 30 (m), but this depends strongly on E_0. Much more large spans (for instance of the order of a kilometer) are attained for a tenth of E_o.

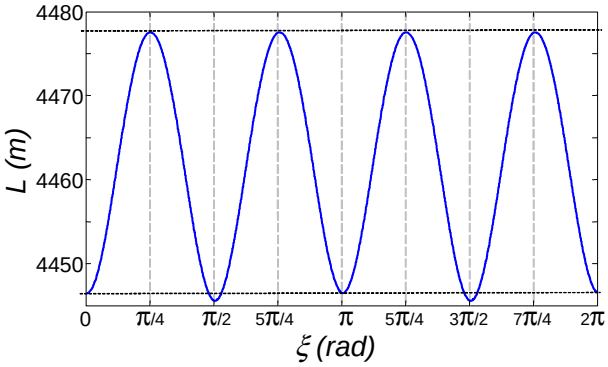

Fig. 5 - Variation of L as a function of ξ

In Fig 6 the estimation of the distance for the point of no return is illustrated in five different cases:

Case I) Optimized velocities without current ($\mathbf{v}_c = \mathbf{0}$)

Case II) Optimized velocities with current

Case III) Velocities obtained in Case I but with current

Case IV) Velocities 50% larger than in Case II

Case V) Velocities 50% lower than in Case II.

For the rectangular meandering path in Fig. 1, bottom, it results a set of four different velocities u_i´s which are described in Table I. Additionally, the elapsed time and the path distance covered bidirectionally is registered in the third and forth columns respectively. Related to this information, Fig. 6 shows the locations of the point of no return in all the cases, and Fig. 7 details of the first three cases.

Table I - Results for the five simulated cases

Case	Velocities (m/s)				Time $(hours)$	L (Km)
	u_1	u_3	u_2	u_4		
I	1.014	1.014	1.014	−1.014	1.27	4.621
II	0.957	0.957	1.099	−1.099	1.22	4.478
III	1.014	1.014	1.014	−1.014	1.22	4.453
IV	1.435	1.435	1.648	−1.648	0.68	3.746
V	0.478	0.478	0.549	−0.549	1.67	3.084

One sees that the elapsed time in the first three cases are very close into each other, although the Case I and II are optimal only. In the nonoptimal Case IV the elapsed time is the lowest one but L is not too large as in optimal cases. The reason for that is the high energy E_m spent to overcome the drag resistance in the motion. On the contrary, in the nonoptimal Case V, this effort is strongly reduced but the exposition time to the current is larger and this spent the available energy inefficiently in the long term.

VII. Conclusions

In this paper the design of an algorithm to real-time planning of the optimal energy consumption in AUVs navigating on structured meandering paths is developed. The proposed algorithm is conceived for missions with gathering of uniformly distributed data on a region of interest in perturbed environments.

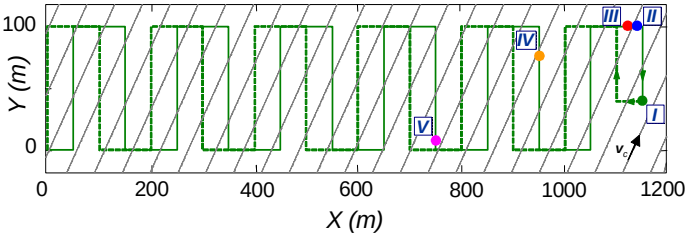

Fig. 6 - Five scenarios for the point of no return: 1) optimized rates with null current, 2) optimized rates with current, 3) path with the optimized rates of 1 but with current, 4) 50%-augmented rates with respect case 2), 5) 50%-reduced rates with respect to case 2

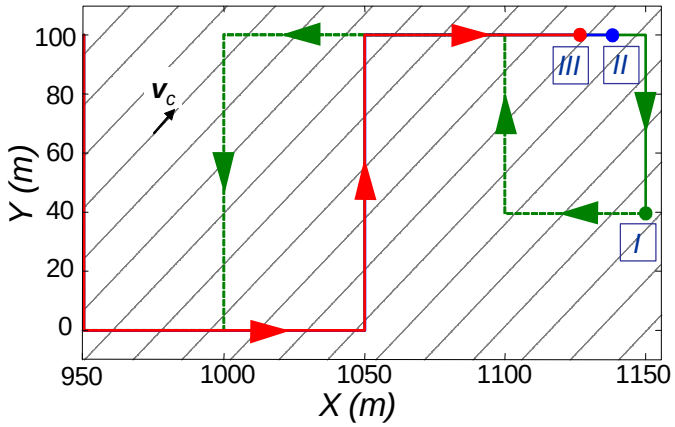

Fig. 7 - Details of the end paths in Cases 1, 2 and 3

The algorithm can be embedded in a control system as an outer loop that provides the optimized geometric trajectory and a set of constant optimal velocities that are taken as rate references along the partial stretches. Transients are assumed to elapse a comparative small time than the stationary kinematics. This assumption is supported by the employment of a high-performance control system.

The optimization procedure has consisted in calculating the location of the most distant point of no return on a bidirectional meandering path by searching for a set of optimal velocities and a suitable orientation for the ultimate path. The calculation of optimal velocities supposed the maximization of the number of partial stretches as well as

the optimal orientation of the whole path. In this way the optimal distribution of spent energies along the partial stretches are determined backwards starting from the end point of the path.

Since the algorithm is timesaving, the optimal solution for the kinematics can be calculated in real-time and restarted whenever changes of the flow field are detected.

Finally, a case study is simulated to illustrate comparative features in optimal and nonoptimal cases.

References

Blidberg R. (2001). The development of autonomous underwater vehicles (AUVs); A brief summary. *Autonomous Undersea Systems Institute Publication*, ICRA, Seoul, Korea.

Chyba, M., Maurer, H., Sussmann, H.J., Vossen, G. (2004). Underwater vehicles: the minimum time problem. *In Proceedings of the 43th IEEE Conference on Decision and Control*, Bahamas.

Chyba, M. and Haberkorn, T. (2005). Autonomous underwater vehicles: singular extremals and chattering. *In Proceedings of the 22nd IFIP TC 7 Conference on System Modeling and Optimization*, Italy.

Chyba, M., Haberkorn, T., Smith, R.N. and Choi, S.K. (2008). Design and implementation of time efficient trajectories for autonomous underwater vehicles. *Ocean Engineering*, 35, 63–76.

Chyba, M., Haberkorn, T., Singh, S.B., Smith R.N.and Choi. S.K. (2009). Increasing underwater vehicle autonomy by reducing energy consumption. *Ocean Engineering*, 36, 62–73.

Fossen, T.I. (1994). *Guidance and control of ocean vehicles*, John Wiley&Sons, New York.

Healey, A.J., Rock, S.M., Cody, S., Miles, D., Brown, J.P. (1995). Toward an improved understanding of thruster dynamics for underwater vehicles. *IEEE Journal of Oceanic Engineering*, 20 (4).

Inzartev A.V.(Ed.) (2009). *Underwater vehicles*, In-Tech, Vienna, Austria.

Jordán M.A. and Bustamante, J.L. (2009). Adaptive control for guidance of underwater vehicles. *In Underwater Vehicles*, In-Tech, Vienna, Austria, A.V. Inzartev (Ed.), Chapter 14, 251-278.

Kruger, D., Stolkin, R., Blum, A. and Briganti, J. (2007). Optimal AUV path planning for extended missions in complex, fast-flowing estuarine environments. *In IEEE International. Conference on Robotics and Automation*, Roma, 4265-4270.

Sarkar, N. and Podder, T.K. (2001). Coordinated motion planning and control of autonomous underwater *vehicle*-manipulator systems subject to drag optimization. *IEEE Journal of Oceanic Engineering*, 26 (2), 228-239.

Woodrow I., Purry, C., Mawby A. and Goodwin, J. (2005). Autonomous Auv Mission Planning And Replanning- Towards True Autonomy. *in 14th International Sym-posium on Unmanned Untethered Submersible Technology*, Durham, NH.

Yang G. and Zhang R. (2009). Path planning of AUV in turbulent ocean environments used adapted inertia-weight PSO. *In Fifth International Conference on Natural Computation*, 299-302.